Theory of Phase Separation in Polymer Nanocomposites

Justin B. Hooper and Kenneth S. Schweizer*

Department of Materials Science and Engineering, University of Illinois, 1304 West Green Street, Urbana, Illinois 61801

Received March 14, 2006; Revised Manuscript Received May 23, 2006

ABSTRACT: The microscopic polymer reference interaction site model theory of polymer nanocomposites composed of flexible chains and spherical nanoparticles has been employed to study second virial coefficients and spinodal demixing over a wide range of interfacial chemistry, chain length, and particle size conditions. For hard fillers, two distinct phase separation behaviors, separated by a miscibility window, are generically predicted. One demixing curve occurs at relatively low monomer−particle attraction strength and corresponds to a very abrupt transition from an entropic depletion attraction-induced phase separated state to an enthalpically stabilized miscible fluid. The homogeneous mixture arises via a steric stabilization mechanism associated with the formation of thin, thermodynamically stable bound polymer layers around fillers. The second demixing transition occurs at relatively high monomer−particle adsorption energy and is inferred to involve the formation of an equilibrium physical network phase with local bridging of particles by polymers. This spinodal is sensitive to both particle−monomer diameter ratio and the spatial range of the interfacial attraction. The miscibility window narrows, and can ultimately disappear, with increasing polymer chain length, direct van der Waals attractions between fillers, and/or particle−monomer size asymmetry ratio. The implications of our results for the design of well-dispersed thermodynamically stable polymer nanocomposites, and the formation of nonequilibrium gels, are discussed.

I. Introduction

Dense polymer−particle mixtures, or polymer nanocomposites, are of major scientific and technological interest.[1−6] Fundamental issues include equilibrium miscibility, dispersion and spatial organization of particles or fillers, particle-induced modification of polymer conformation and packing, structure of the polymer−particle interface, and the consequences of all these considerations on thermomechanical properties in the fluid and nonequilibrium glass or gel states. Diverse theoretical and simulation approaches have begun to be employed to study elementary aspects of model polymer−particle mixtures.[7−17] However, severe computational difficulties associated with equilibration and an exceptionally wide range of relevant length and time scales have largely prevented exploration of the equilibrium phase behavior and the role of realistic particle−monomer size ratio, strong polymer−filler attractions, and long entangled chains.

Recently, we employed the microscopic polymer reference interaction site model (PRISM) integral equation theory[18] to investigate structure, effective forces, and thermodynamics in entropy-controlled *athermal* mixtures in the one- and two-particle limit.[19] The influence of particle size, degree of polymerization, and melt density has been established. In concentrated solutions and melts, there exist oscillatory depletion forces between two hard spheres due to monomer-level packing correlations. The corresponding potential of mean force generally exhibits extremely large attractive interactions at contact. The key geometric variable is the ratio of particle diameter to monomer diameter. The presence of strong polymer-mediated contact attractions between particles suggests that purely athermal mixtures are macroscopically phase separated in equilibrium. Hence, as long appreciated in the practical filled polymer composite field,[1,4] attractive interactions between polymer and particle are required to achieve some degree of miscibility or dispersion.

* Corresponding author. E-mail: kschweiz@uiuc.edu.

Most recently, a detailed computational PRISM study of the pair correlation function and potential of mean force (PMF) between a pair of spherical particles dissolved in an *adsorbing* homopolymer melt has been performed.[20] The additional roles of the strength and spatial range of monomer−particle attractions and direct interfiller attractions have been established. For hard-sphere fillers, four general categories of polymer-mediated nanoparticle organization are found: contact aggregation due to depletion attraction, segment-level tight particle bridging, steric stabilization due to thermodynamically stable "bound polymer layers", and "telebridging", where distinct adsorbed layers coexist with longer-range bridging. As the direct interparticle attractions increase in strength, the globally stable bridging configuration is gradually destabilized and replaced by contact aggregation as the most favored state of packing. However, bridging states often remain as metastable local minima of the PMF. Mixtures in the steric stabilization category are much less affected by interfiller attractions due to the thermodynamic stability of distinct bound polymer layers. These theoretical studies have also suggested the interesting possibility that sterically stabilized nanofillers may crystallize in a homopolymer matrix at relatively low volume fractions, and the PMF calculations have implications for nonequilibrium gelation or filler network formation and kinetic stabilization via large repulsive barriers.[20]

The purpose of the present paper is to build on our prior work to treat a key thermodynamic property (particle second virial coefficient) and phase separation. Two types of phase separation are found, one mediated by depletion attraction and contact aggregation of fillers, and a second induced by local bridging of fillers resulting in the formation of a polymer−particle complex. For specific ranges of system variables, a novel miscibility window is predicted corresponding to a compromise state of spatial organization where relatively thin and distinct bound layers form around fillers.

The remainder of the paper is structured as follows. In Section II, we briefly review the model, theory, and results of prior work.

10.1021/ma060577m CCC: $33.50
Published on Web 06/30/2006

A systematic study of the filler second virial coefficients is given in Section III. Section IV presents our primary phase diagram results for hard-sphere fillers. The effect of direct interparticle van der Waals attractions on miscibility is considered in Section V. The paper concludes with a summary and discussion.

II. Theory and Model

A. Chain Model and Attractive Interactions. Polymers are treated as athermal chains of N spherical interaction sites, or monomers, of diameter d that interact via pair-decomposable hard core potentials. A freely jointed chain (FJC) model is adopted with a rigid bond length $l = 4d/3$ (corresponding to a persistence length of 4/3), and $d \equiv 1$ is the polymer segment diameter which is the unit of length. The FJC structure factor is:[21]

$$\omega_p(k) = (1 - f)^{-2}[1 - f^2 - 2N^{-1}f + 2N^{-1}f^{N+1}] \quad (1)$$

where $f = \sin(kl)/kl$. The FJC chain model ignores nonideal conformational effects, which are expected to be minor for the melt conditions of interest. In principle, filler perturbation of polymer conformation at nonzero volume fractions could be treated based on the fully self-consistent version of PRISM theory, which involves the construction of a medium-induced solvation potential and solution of an effective single-chain problem with Monte Carlo simulation.[18] The accuracy of this approach for polymer nanocomposites, particularly when the monomers are strongly attracted to the fillers, is not known. However, the few existing experiments and simulations for dense polymer nanocomposites at finite filler loadings suggest that conformational perturbations are small or negligible.[6−14] Most importantly for the present work is that, because our focus is the dilute filler limit, within the liquid-state theory approach the statistical conformations are not perturbed. Fillers are modeled as rigid spheres of diameter D, which have a trivial single-particle structure factor, $\omega_c(k) \equiv 1$.

Given the system-specificity of the attractive branch of real interaction potentials and our adoption of a (moderately) coarse-grained polymer model, a minimalist two-parameter monomer−particle attraction of an exponential form is utilized. It is defined by the strength at contact, ϵ_{pc}, and a spatial range parameter α,

$$U_{pc}(r) = -\epsilon_{pc} \exp\left[-\frac{r - \sigma_{pc}}{\alpha d}\right] \quad (2)$$

where $\sigma_{pc} = (D + d)/2$. For real materials, the magnitude of ϵ_{pc} can vary from "weak" (a fraction of a k_BT) to strong (several k_BT). Throughout the paper, ϵ_{pc} and all other energies are in units of the thermal energy. The spatial range parameter α is also material-dependent and within a coarse-grained chain model will depend on the Ångstrom-scale chemical details that have been averaged over, e.g., monomer size and shape. For a chemically specific type attraction, the range can be significantly smaller than the size of a coarse-grained monomer. As previously discussed,[20] different values of α mimic the different types of intermolecular attractions experienced in real systems. For low values of α ($\sim$0.25), the model mimics specific chemical types of attractions such as charge transfer or hydrogen bonding. Moderate values ($\alpha \sim 0.5$) are representative of generic dispersive Lennard-Jones (LJ) or van der Waals attractions. Even higher values of α ($\sim$1.0) are relevant when the coarse-grained monomers contain a relatively large number of elementary units. Negative values of ϵ_{pc} are not studied because they correspond to a dewetting situation where phase separation is both enthalpically and entropically favored.

As described in depth elsewhere,[20] the basic form of eq 2 is consistent with the even more realistic "composite particle" model of Henderson and co-workers,[22] which we refer to as the colloid Lennard-Jones (CLJ) potential. In the CLJ model, two spheres, i and j, of different diameters, d_i and d_j, are each composed of elementary units of diameter b interacting via a 6−12 LJ potential with energy parameter E_{ij}. The net interaction between the two composite spheres is a pairwise sum over LJ potentials holding the interparticle separation fixed. The discrete sums are converted to volume integrals corresponding to adopting a continuous distribution of the elementary units.[22] In contrast with standard continuum models in colloid science,[23,24] the inclusion of (and integration over) the repulsive portion of the LJ potential prevents any unphysical divergence of the attractive interactions when the two particles are in contact.

The full CLJ potential is a complicated, but known,[22] function of all the relevant variables (E_{ij}, d_i, d_j, b). When applied to the monomer−particle interaction where $b < d \ll D$, the attractive minimum energy is

$$\epsilon_{pc} \approx E_{pc}d/2b \quad (3)$$

which is independent of D because the particle appears as a "wall or surface" to the much smaller monomer. For direct particle−particle attractions, we employ the attractive branch of the full CLJ potential,[20,22] which is characterized by its strength at contact

$$\epsilon_{cc} \approx E_{cc}D/4b \quad (4)$$

Note that ϵ_{cc} scales linearly with particle diameter, and E_{cc} and E_{pc} are the LJ potential parameters for the elementary units (size b) that compose the monomer and particle. For example, a CH_2 group corresponds to $b \sim 3-4$ Å and $E/k_B \sim 40$ K. We note that some real nanoparticle fillers have directional interactions and such anisotropy is not addressed by our CLJ model.

B. PRISM Theory. PRISM theory has been previously shown to describe quite well the physical behavior of a number of different systems (suspensions and melts) composed of hard spherical particles and flexible linear chains.[19,20,25−31] For dense polymer nanocomposites, conformational changes are expected to be small due to the short spatial range of the density−density fluctuation correlation length in melts.[32] Nonlocal conformational entropy effects, of paramount importance in dilute polymer solutions,[26] are highly screened for a nearly incompressible melt. Hence, the local site−site Percus−Yevick (PY) closure[18,33,34] is quite accurate for monomer−monomer and monomer−particle direct correlation functions. However, for dilute spheres in a dense polymer matrix, nonlocal effects associated with a large particle diameter to monomer diameter ratio, D/d, are important, and the appropriate closure[19] for the particle−particle direct correlation function is the hypernetted chain (HNC) approximation.[34]

The technical details of the polymer nanocomposite version of PRISM theory have been discussed in depth previously.[19,20] By treating all sites on a chain as statistically equivalent, the matrix site−site Ornstein−Zernike-like equations in Fourier space are given by,[18,33]

$$h_{ij}(k) = \omega_i[C_{ij}(k)\omega_j + \sum_l C_{il}(k)\rho_l h_{lj}(k)] \quad (5)$$

where $h_{ij}(r) = g_{ij}(r) - 1$ is the nonrandom part of the intermolecular site−site pair correlation function between species i and j, $C_{ij}(r)$ is the corresponding intermolecular direct

correlation function, $\omega_i(k)$ is the single-molecule structure factor of species i, and ρ_l is the site number density of species l.

In the infinitely dilute particle limit of present interest, $\rho_p d^3$ is the only relevant density, and eq 5 reduces to three uncoupled, sequentially solvable integral equations:[19,20]

$$h_{pp}(k) = \omega_p(k)C_{pp}(k)[\omega_p(k) + \rho_p h_{pp}(k)] \equiv \omega_p(k)C_{pp}(k)S_{pp}(k) \quad (6)$$

$$h_{cp}(k) = C_{cp}(k)S_{pp}(k) \quad (7)$$

$$h_{cc}(k) = C_{cc}(k) + \rho_p C_{cp}^2(k)S_{pp}(k) \quad (8)$$

The pure polymer fluid structure factor is defined in eq 6. Hard-core interactions imply the exact impenetrability conditions:

$$g_{ij}(r) \equiv 0, \qquad r < \sigma_{ij} \quad (9)$$

where σ_{ij} is the distance of closest approach between sites of type i and j. Closure relations outside the hard core are required. The site−site PY approximation[18,33] is adopted for the polymer−polymer (PP) and polymer−particle (PC) direct correlations:

$$C_{ij}(r) = (1 - e^{\beta U_{ij}(r)})g_{ij}(r), \qquad r > \sigma_{ij} \quad (10)$$

where U_{ij} is the site−site interaction potential. The HNC closure is utilized for the $r > \sigma_{cc}$ particle−particle (CC) direct correlations:[33,34]

$$C_{cc}(r) = h_{cc}(r) - \ln g_{cc}(r) - \beta U_{cc}(r), \qquad r > \sigma_{cc} \quad (11)$$

Prior work for athermal systems has demonstrated that PRISM theory with the above closures accurately captures all features of the polymer-induced interaction of two nanoparticles in dense melts.[19]

In the present work, all calculations are performed at a total packing fraction of 0.4, which corresponds to a typical dense melt value with a realistic dimensionless compressibility.[18−20] The integral equations are solved with the iterative Picard method.[34]

C. Filler Potential of Mean Force. The complex consequences of both interfacial (polymer−nanoparticle) and direct (nanoparticle−nanoparticle) attraction on structural correlations at the two-particle level have very recently been studied.[20] To gain a physical understanding of the new phase separation results requires briefly reviewing our prior structural studies.

The structure of the model polymer nanocomposites reflects a balance between two very different competing effects. One limit is the entropically dominated athermal system, where oscillatory depletion attractions favor contact particle aggregation. The other limit is an enthalpically dominated mixture, where the addition of strong attractive interactions between the filler and monomers results in thin layers of polymer strongly associating with, or adsorbing onto, the particles. The resulting particle−particle potential of mean force favors well-defined, small interparticle separations, i.e., local "bridging". Between these two extremes is a third behavior, in which a polymer gains enough cohesive interaction energy to associate with a single filler, but not enough to give up the additional entropy required for association with multiple particles. In this case, a nanoparticle is surrounded by a *thermodynamically* stable "bound" polymer layer, typically on the order a few monomer diameters thick, which sterically stabilizes the particles in the polymer matrix.[20]

Figure 1 presents an overview of the different forms of the polymer-mediated potentials of mean force (PMF) between two hard sphere particles and schematically indicates the corresponding nanoparticle organization.[19,20] In general, four distinct cases occur depending on the parameters of the exponential monomer−particle attractive pair potential of eq 2: the monomer−particle attraction range (α in units of d) and strength at contact (ϵ_{pc}, in units of thermal energy, k_BT). For all α, at low enough ϵ_{pc}, all systems exhibit contact particle aggregation (Figure 1, I). This is the effectively athermal, entropy-dominated extreme. For intermediate values of ϵ_{pc}, one of two behaviors emerges depending upon the value of α. At low α ($0 < \alpha \leq 0.5$), a transition is seen from contact aggregation to bridging, where nanoparticles aggregate at a specific (α-dependent) distance (Figure 1, II). For larger α, corresponding to a spatially longer-range polymer−particle attraction and, hence, a higher interfacial cohesive energy at constant ϵ_{pc}, a bound polymer layer of 2−3 monomer diameters forms around the nanoparticle, resulting in net repulsion between the fillers (Figure 1, III). Finally, for the higher α and sufficiently large ϵ_{pc}, the tendency for particles to be sterically stabilized is overcome by the longer-ranged strong attractions between polymer and fillers, and the system becomes "telebridged" (Figure 1, IV). The latter jargon implies a state of organization similar to bridging in the low-α system (Figure 1, II) but at a larger interparticle distance, with bridging superimposed on a remnant bound layer characteristic of sterically stabilized systems (Figure 1, III).

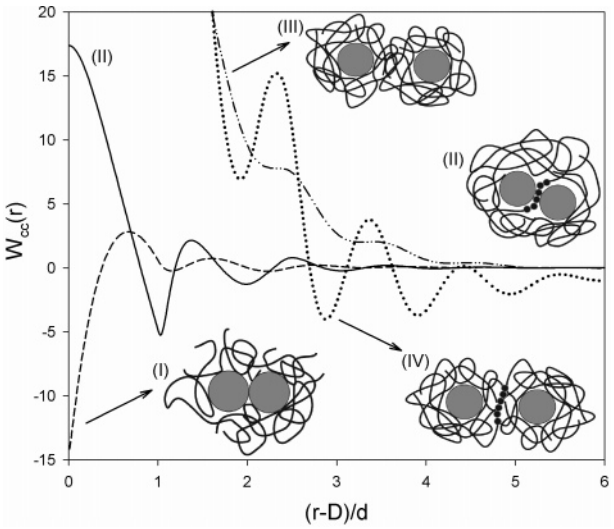

Figure 1. Representative examples of the particle−particle potential of mean force for systems with $D/d = 16$ and $N = 100$ which exhibit the four different types of organization: (I) Contact aggregation/fluid−fluid phase separation ($\alpha = 0.25$, $\epsilon_{pc} = 0.25$, dash), (II) bridging ($\alpha = 0.25$, $\epsilon_{pc} = 2.25$, solid), (III) steric stabilization ($\alpha = 1.0$, $\epsilon_{pc} = 2.0$, dash−dot−dot), and (IV) telebridging ($\alpha = 1.0$, $\epsilon_{pc} = 3.0$, dotted). Schematics of favored particle configurations are indicated.

D. Spinodal Phase Separation. The spinodal demixing criterion of a multicomponent system is:[18,34]

$$\lim_{k\to 0} S_{ij}(k) = \infty \quad (12)$$

for *all* i and j. Here, $S_{ij}(k)$ is a partial structure factor or Fourier transform of the real-space collective density fluctuation correlation function associated with species i and j. This condition is equivalent to vanishing of the determinant of the matrix of second derivatives of the free energy:

$$\det(\underline{S}^{-1}) = \det(\underline{I} - \underline{\Omega C}) = 0 \quad (13)$$

where $\underline{I}$ is the identity matrix, $\underline{\Omega}$ is a diagonal matrix with components $\Omega_{ii} \equiv \rho_i\omega_i$, and $\underline{C}$ is the matrix of direct correlation

functions. For a single-component fluid, eq 13 reduces to the scalar expression:[18,34]

$$S^{-1}(k=0) \equiv N^{-1} - \rho C(k=0) = (\rho k_B T \kappa)^{-1} = 0 \quad (14)$$

where ρ is the site number density, and κ the isothermal compressability. For the two-component system of present interest, eq 13 yields the spinodal stability condition:[18]

$$\Lambda = N^{-1} - \rho_p \tilde{C}_{pp} - \rho_c N^{-1} \tilde{C}_{cc} + \rho_p \rho_c (\tilde{C}_{pp}\tilde{C}_{cc} - \tilde{C}_{pc}^{\,2}) \equiv 0 \quad (15)$$

where $\tilde{C}_{ij} \equiv C_{ij}$ $(k = 0)$ and ρ_p (ρ_c) is the monomer (particle) number density.

While eq 15 is exact for our compressible mixture, it requires numerical solution of the three coupled integral equations 6−8. For dense mixtures with a large size asymmetry, convergence is often extremely difficult or impossible. Hence, for both computational simplicity and conceptual clarity, we determine the spinodal curves perturbatively in particle density by expanding the terms of eq 15 through lowest nontrivial order in ρ_c. Inspection of eq 15 reveals only the infinite dilution ($\rho_c \equiv 0$) values of $\tilde{C}_{cc}$ and $\tilde{C}_{pc}$ are then needed. However, evaluation of the polymer contributions requires both the infinite dilution value, $\tilde{C}_{pp}$, and an additional first-order correction to the polymer direct correlation function associated with lowest-order polymer−particle interactions. Physically, the latter describes particle-induced changes in polymer−polymer correlations. Hence:

$$\tilde{C}_{pp}(\rho_c) = \tilde{C}_{pp}(\rho_c \to 0) + \rho_c \Delta C_{pp} \equiv C_{pp}^{\,0} + \rho_c \Delta C_{pp} \quad (16)$$

$$\tilde{C}_{pc}(\rho_c) = \tilde{C}_{pc}(\rho_c \to 0) \equiv C_{pc}^{\,0} \quad (17)$$

$$\tilde{C}_{cc}(\rho_c) = \tilde{C}_{cc}(\rho_c \to 0) \equiv C_{cc}^{\,0} \quad (18)$$

where the first-order correction to the polymer direct correlation function is $\Delta C_{pp} = (\partial \tilde{C}_{pp}/\partial \rho_c)|_{\rho_c \to 0}$.

By using eqs 16−18, the spinodal boundary of eq 15 can now be written as:

$$0 = 1 - \rho_c \rho_p \tilde{S}_{pp} \Delta C_{pp} + 2\rho_c B_{2,cc} \quad (19)$$

where $\tilde{S}_{pp} \equiv S_{pp}^{\,0}$ $(k = 0)$, and the particle second virial coefficient $B_{2,cc}$ consists of both "direct" and "indirect" (polymer-mediated) contributions:

$$2B_{2,cc} = -h_{cc}(k=0) = -(C_{cc}^{\,0} + \rho_p \tilde{S}_{pp} (C_{pc}^{\,0})^2) \quad (20)$$

There are three distinct contributions to the spinodal boundaries, as illustrated schematically in Figure 2. The first two involve the polymer matrix: (a) $\tilde{S}_{pp}$, the dimensionless isothermal compressibility of the *unperturbed* polymer melt, and (b) the first-order correction, ΔC_{pp}, which quantifies the leading order modification of contribution (a) upon addition of particles to the polymer melt. The remaining contribution (c) is due to both direct and polymer-mediated components of the particle−particle second virial coefficient in eq 20.

By utilizing eqs 19 and 20, the spinodal boundary can be written as a critical filler volume fraction ($\phi \equiv \rho_c D^3/\bar{\rho}$):

$$\phi_c = \frac{\bar{\rho}\bar{C}_{pp} - 1}{\bar{\rho}\left[\bar{C}_{pp} + \bar{C}_{cc} - \bar{\rho}(\bar{C}_{pp}\bar{C}_{cc} - \bar{C}_{pc}^{\,2}) - \dfrac{\partial \bar{C}_{pp}}{\partial \phi}\right]} \quad (21)$$

where $\bar{\rho} = \rho_p N d^3 + \rho_c D^3 \equiv 6\eta/\pi$ is the total reduced site density,

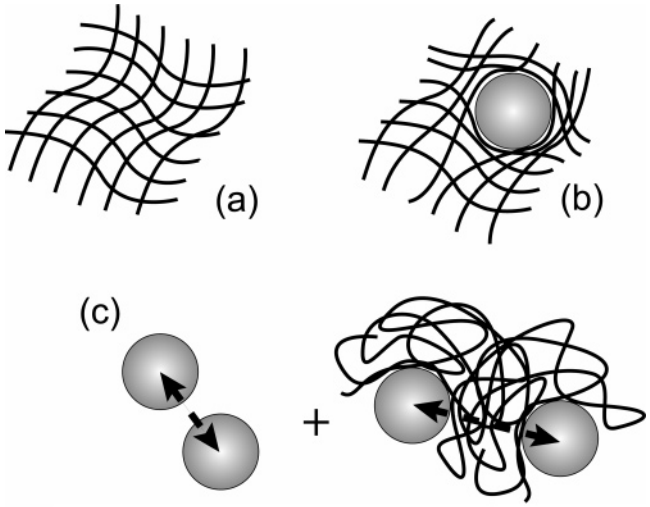

Figure 2. Schematic representation of the thermodynamic factors that determine spinodal phase separation in the low nanoparticle concentration limit. (a) Monomer−monomer entropic packing effects that determine the compressibility of the pure polymer matrix. (b) Changes in the polymer free energy due to the insertion of a nanoparticle in the polymer melt. (c) The B_2 (second virial) level interaction between nanoparticles due to both direct dispersion interactions (when present) and the polymer-induced correlations.

η is the overall packing fraction, $\bar{C}_{pp} \equiv \tilde{C}_{pp}/d^3$, $\bar{C}_{cc} \equiv \tilde{C}_{cc}/D^3$, and $\bar{C}_{pc}^{\,2} \equiv \tilde{C}_{pc}^{\,2}/d^3D^3$. Although eq 21 is only rigorous perturbatively in particle concentration, we employ it as a zeroth-order estimate of spinodal phase boundaries at nonzero particle volume fractions. We expect the resulting phase boundaries will be at a minimum qualitatively reliable.

An even simpler approach to investigating phase behavior invokes a further approximation that the particle-related contributions dominate. By discarding the explicit polymeric contributions in eq 19, the spinodal demixing condition becomes one of an *effective* one-component (E1C) system form:

$$\phi_c = -(8\bar{B}_2\eta)^{-1} \quad (22)$$

where $\bar{B}_2 = B_{2,cc}/B_{2,HS}$, and $B_{2,HS} = 2\pi D^3/3$ is the second virial coefficient of a hard-sphere reference system. This reduction is a literal second virial analysis of spinodal phase separation for a one-component particle fluid that interacts via the polymer-mediated PMF. One reason one might expect this simplification to be accurate is the low dimensionless compressibility of a dense mixture (i.e., small value of $\tilde{S}_{pp}$ in eq 19). If one denotes this PMF for *hard-sphere* fillers as $W_{cc,HS}$, then the total PMF in the presence of direct interparticle interactions (U_{cc}) is simply given by:

$$W_{cc}(r) = W_{cc,HS}(r) + U_{cc}(r) \quad (23)$$

and $g_{cc}(r) = e^{-\beta W_{cc}(r)}$. Equation 22 then follows from the effective one-component analogue of eq 15, where the second virial coefficient is:

$$B_{2,cc} = -\frac{1}{2}\int d\mathbf{r} h_{cc}(r) = -\frac{1}{2}\int d\mathbf{r}(e^{-\beta W_{cc}(r)} - 1) \quad (24)$$

This approach allows relatively rapid investigation of spinodal phase behavior by reducing the problem to computing the PMF between two hard particles, with direct particle interactions trivially appended. Such an effective second virial coefficient approach has been widely applied in protein solution phase-

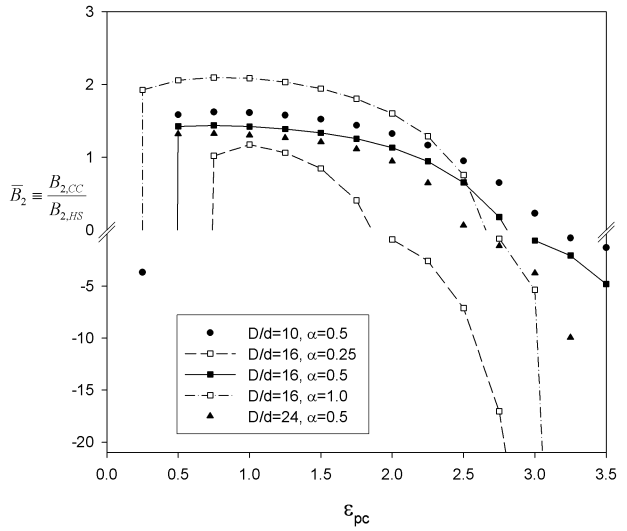

Figure 3. Normalized second virial coefficient $\bar{B}_2$ of hard spheres ($\epsilon_{cc} = 0$) as a function of ϵ_{pc} for several size asymmetry ratios D/d (symbols) and interfacial attraction ranges α (lines) for $N = 100$. Specific cases shown are $D/d = 10$, 16, and 24 (circle, square, and triangle, respectively) and $\alpha = 0.25$, 0.5, and 1.0 (dash, solid, and dash−dot, respectively). The lines are a guide to the eye, and for clarity, the symbols for different size asymmetry ratios at constant $\alpha = 0.5$ are filled. Note the change of scale of the ordinate for $\bar{B}_2 < 0$.

behavior studies and empirically is found to often describe experiments reasonably well even when the protein concentration is not small.[35−38]

III. Second Virial Coefficients

Figure 3 shows dimensionless second virial coefficients, $\bar{B}_2$, for a variety of hard filler systems of variable size asymmetry ratio (D/d), monomer−particle attraction range (α), and interfacial attraction strength (ϵ_{pc}) at a fixed $N = 100$. For the $\epsilon_{pc} = 0$ athermal case (not plotted), there is a large and negative $\bar{B}_2$ due to the extremely strong depletion attraction; for example, $\bar{B}_2 = -2.5 \times 10^3$, -1.25×10^6, -7.58×10^9 for $D/d = 10$, 16, 24, respectively. As polymer−particle attractions are turned on, there is an abrupt ($\epsilon_{pc} \leq 1$ for all α investigated) change to a net repulsive, positive $\bar{B}_2$, indicative of steric stabilization behavior. All systems exceed the threshold of $\bar{B}_2 = 1$, indicating an enhanced repulsion relative to bare hard spheres. The ϵ_{pc} value at which this occurs monotonically decreases as α (D/d) increases (decreases) and can be significantly less than k_BT. The α dependence is a consequence of the larger interfacial cohesive energy (at constant ϵ_{pc}) with increasing spatial range of the monomer−filler attraction. The size asymmetry ratio trend of a smaller repulsive $\bar{B}_2$ for larger particles reflects both the relatively smaller enhancement of the filler effective diameter due to polymer adsoption and the less effective stabilization at a given value of ϵ_{pc} due to the larger magnitude of the initial depletion attraction that must be overcome. At the PMF level, the latter scales linearly with D/d.[19,20]

As the interfacial attraction is further increased, one sees from Figure 3 that nonmonotonic, α-dependent changes of $\bar{B}_2$ occur. For the shortest-ranged ($\alpha = 0.25$) interaction, $\bar{B}_2$ very quickly becomes attractive again. In contrast, the longest-range ($\alpha = 1$) system requires significantly more interfacial cohesion before $\bar{B}_2 < 0$. The $\alpha = 0.5$ intermediate range attraction system remains surprisingly stable ($\bar{B}_2 > 0$) over the largest range of ϵ_{pc} studied due to a subtle competition between packing entropy and interfacial attraction considerations. For the shortest-ranged ($\alpha = 0.25$) attraction, the system quickly adopts a bridging type

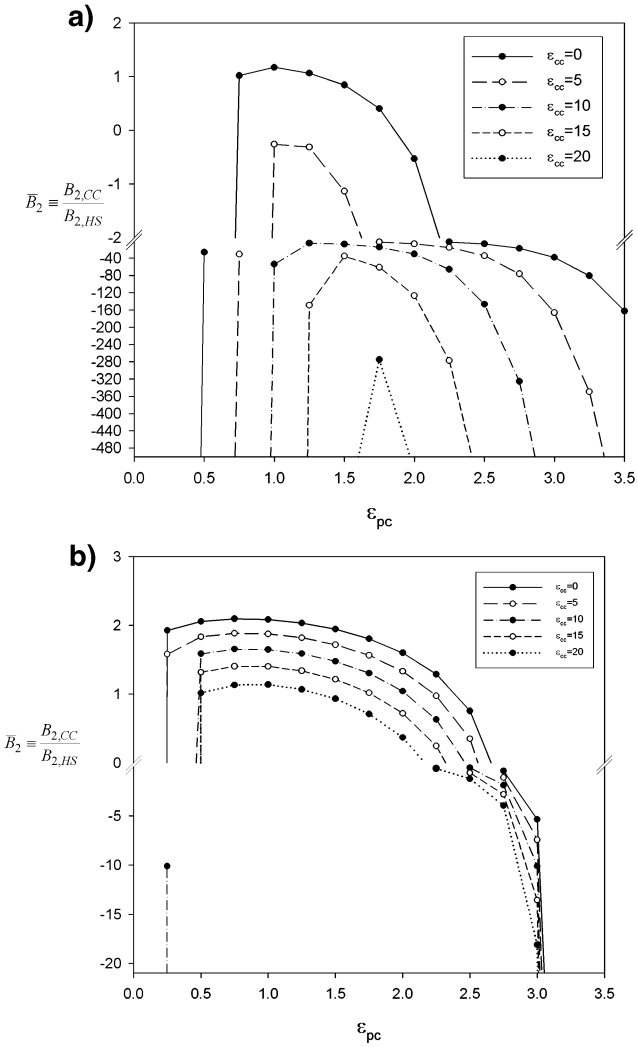

Figure 4. (a) Effect of direct van der Waals nanoparticle attractions on the normalized particle second virial coefficient, $\bar{B}_2$, for a system with $D/d = 16$, $N = 100$, and $\alpha = 0.25$. The absolute nanoparticle attraction at contact in units of k_BT: $\epsilon_{cc} = 0.0$, 5.0, 10.0, 15.0, and 20.0 (solid, long dash, dash−dot, short dash, and dotted, respectively). Symbols are the calculations, while the lines are a guide to the eye. Note the change of scale of the ordinate for $\bar{B}_2 < -2$. (b) Effect of direct nanoparticle attractions on the normalized particle second virial coefficient. All variables are the same as in (a), except $\alpha = 1$. Note the change of scale of the ordinate for $\bar{B}_2 < 0$.

of organization, and subsequent increases in ϵ_{pc} reinforce this strong bridging attraction. Conversely, for the longest-range ($\alpha = 1$) case, a diffuse, yet relatively large, bound layer of monomers initially emerges due to the soft attraction.[20] As ϵ_{pc} increases, this layer compresses until some critical ϵ_{pc} is reached, at which point the system converts to the strongly attracting "telebridging" state.[20] For the intermediate range ($\alpha = 0.50$) attraction, however, a compromise behavior occurs where, even at high attraction energy, the system remains stable.

As expected, Figure 4 shows that the addition of direct nanoparticle attractions ($\epsilon_{cc} > 0$) causes $\bar{B}_2$ to dramatically change. For the shortest-range polymer−particle attraction systems, which display little stabilization for hard spheres, the presence of an attraction between the particles completely destabilizes the system, resulting in $\bar{B}_2 \ll 0$ (Figure 4a). Only in the absence of nanoparticle attractions ($\epsilon_{cc} = 0$) is enhanced repulsive behavior found ($\bar{B}_2 > 1$). As $\epsilon_{cc} > 10$, $\bar{B}_2 < 0$ for all values of ϵ_{pc}, indicating that the relative stabilization associated with polymer adsorption is easily overcome by direct dispersive attractions between particles. On the other hand, for the long-

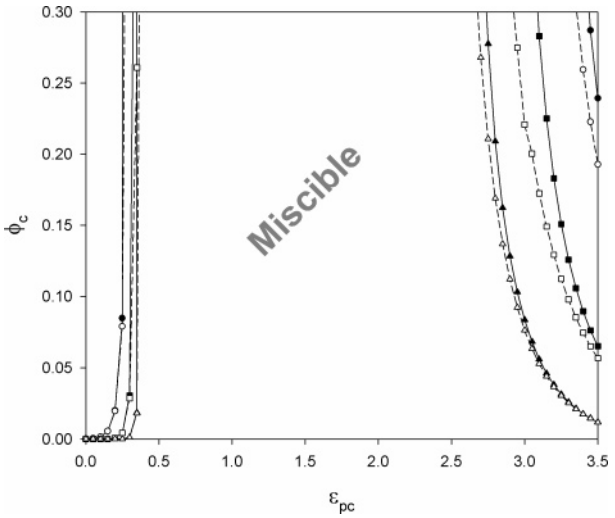

Figure 5. Comparison of spinodal phase-separation boundaries based on the effective one-component second-order virial approach (solid lines) and the full lowest-order theory (dashed lines) for hard-sphere systems with $\alpha = 0.5$, $N = 100$ and $D/d = 10$, 16, 24 (circles, square, triangle, respectively). The lines serve as a guide to the eyes. The central region bounded by the curves represents a miscibility window.

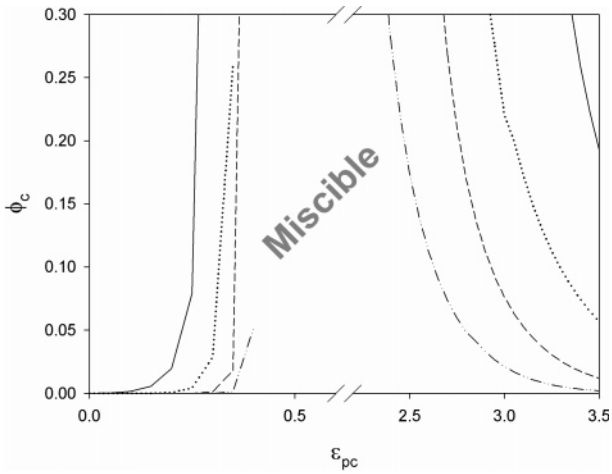

Figure 6. Nanoparticle volume fraction at the spinodal as a function of interfacial attraction strength for a hard-sphere system with $\alpha = 0.5$, $\epsilon_{cc} = 0.0$, $N = 100$, and $D/d = 10$ (solid), 16 (dotted), 24 (dashed), and 32 (dash−dot−dot). The miscible region between $\epsilon_{pc} \approx 0.5$ and $\epsilon_{pc} \approx 2.25$ has been omitted from the graph.

ranged interfacial attractions in Figure 4b, the steric stabilization associated with bound polymer layers results in tremendous stability in the sense that $\bar{B}_2 > 1$ for a significant fraction of the ϵ_{pc} parameter range studied. Large ϵ_{pc} and ϵ_{cc} are required to induce $\bar{B}_2 < 0$. For stronger direct particle−particle attractions ($\epsilon_{cc} > 10$), contact aggregation and a strongly negative B_2 persists to larger values of ϵ_{pc}, although modest interfacial cohesion ($\epsilon_{pc} > 0.5$) still suffices to overcome filler aggregation. Hence, the system remains stable with $\bar{B}_2 > 1$ for a large portion of the ϵ_{pc} range, ultimately becoming attractive again at very high ϵ_{pc} as telebridging becomes prominent.[20]

Although we do not show more plots, at high monomer−particle attractions the second virial coefficient decreases with polymer degree of polymerization. This follows from our prior finding[20] that the bridging minima deepen with N. However, this is a rather modest effect, and the N-dependence is of a finite size nature in the sense B_2 saturates at a limiting long-chain value. The precise value of N that represents the asympototic limit depends on the specific material parameters. However, typically, we find saturation is essentially achieved by $N = 1600$.

The reduced second virial coefficient can be used to estimate spinodal phase boundaries based on the effective one-component fluid approximation. This approach ignores free energy changes associated with perturbations of the polymer melt by particles, the accuracy of which is not a priori obvious. However, as Figure 5 demonstrates, the E1C description based on eq 22 does quite well at capturing the full spinodal curves that follow from eq 21. It quantitatively and universally overestimates the maximum nanoparticle solubility by a variable amount but is within a factor of ~2 or less of the results of eq 21 for all cases investigated. For the remainder of the paper, all spinodal curves are computed on the basis of the more accurate approach of eq 21.

IV. Effect of Interfacial Cohesion on Phase Behavior

Figure 5 quantifies the phase behavior suggested by the reduced virial coefficients of Figures 3 and 4. The representation chosen is filler volume fraction versus monomer−particle attraction strength nondimensionalized by the thermal energy. Hence, the latter can be experimentally varied by changing filler and/or polymer chemistry or temperature. As a function of polymer−particle attraction strength, the mixture undergoes two phase transitions whose boundaries define a miscibility window. Because we have only computed spinodal instability curves, precise identification of the nature of the coexisting phases cannot be rigorously achieved. However, given the close agreement of the full second virial analysis and the E1C results, and the fact that the latter are fully determined by the particle PMF studied in depth previously[20] and illustrated in Figure 1, educated guesses concerning the nature of the coexisting phases can be made. The first phase transition occurs at low ϵ_{pc} for all system parameters. Physically, it represents classic fluid + fluid phase (F + F) separation driven by polymer-mediated contact depletion aggregation resulting in the coexistence of a polymer-rich and a particle-rich phase. The nature of the coexisting phases for the second transition, indicated by the spinodal boundary at relatively high ϵ_{pc}, is less obvious. However, from the PMF results of Figure 1 and elsewhere,[20] at high ϵ_{pc} it is clear that tight bridging is the favored state of organization. This suggests the demixed state involves a dense networked phase where nanoparticles and polymers are in strong contact. We caution the reader that a precise meaning of our jargon "networked phase" has not been established in terms of standard phase-separation concepts and the construction of a binodal. The general features of the sequence of F + F to miscible to demixed network phase with increasing ϵ_{pc} are seen universally for all combinations of system variables investigated. Quantitative changes in the location of phase boundaries and miscibility window width are introduced by variations of particle diameter, polymer chain length, and chemistry controlled variables (interfacial and direct particle attractions). The sequence of phase behaviors with increasing ϵ_{pc}/k_BT can be thought of in a traditional manner as indicating an entropy-driven lower critical solution temperature (LCST) type of phase separation and an enthalpy-driven upper critical solution temperature (UCST) type of phase separation separated by a miscibility window.

A. Size-Related Effects. We now describe in detail the parametric trends found for the two phase boundaries. Previous work has demonstrated that, beyond a minimal size asymmetry ratio of $D/d \geq 5-6$, the magnitude of both the contact depletion and the bridging/telebridging attractions of the PMF scale linearly with particle size.[19,20] As can be seen in Figures 5 and 6, this explains the narrowing of the miscibility window as the filler−monomer size asymmetry ratio (D/d) grows. For all but

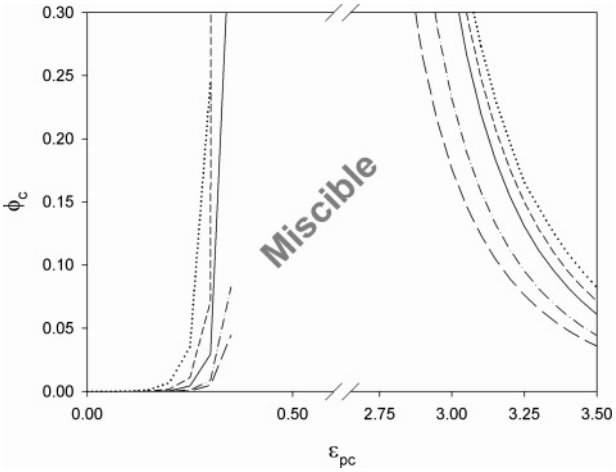

Figure 7. Nanoparticle volume fraction at the spinodal as a function of interfacial attraction strength for a hard sphere system with $D/d = 16$, $\alpha = 0.5$, $\epsilon_{cc} = 0$, and $N = 25$ (dotted), 50 (short dash), 100 (solid), 400 (dash−dot), and 1600 (long dash). The region of miscibility between $\epsilon_{pc} \approx 0.5$ and $\epsilon_{pc} \approx 2.75$ has been omitted from the graph.

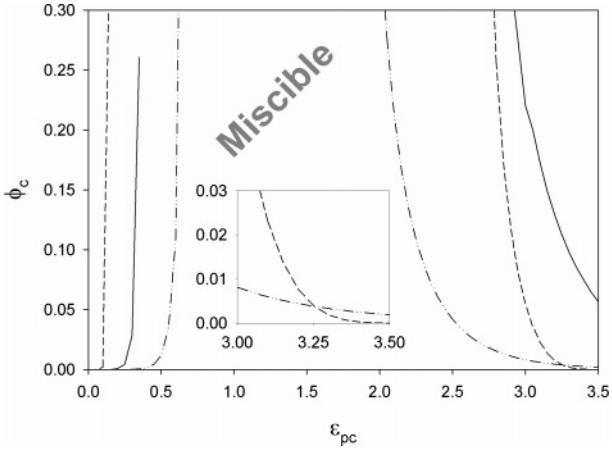

Figure 8. Nanoparticle volume fraction at the spinodal as a function of interfacial attraction strength for a hard sphere system with $D/d = 16$, $\epsilon_{cc} = 0.0$, $N = 100$, and $\alpha = 0.25$ (dash−dot−dot), 0.5 (solid), 1.0 (dash). The inset highlights the high ϵ_{pc} region where there is a curve crossing of the spinodal boundaries of the shortest- and longest-range attraction systems.

the smallest D/d investigated, changes in nanoparticle size have a rather modest effect on the location of the low ϵ_{pc}, F + F spinodal boundary. This is understandable because, at low interfacial attraction, strong entropy-driven depletion attraction causes nanoparticle clustering. As monomer−particle interfacial attraction is increased, a sharp (except for the smallest particles) transition or crossover occurs from the system not having enough interfacial cohesive energy to overcome the depletion aggregation to having sufficient enthalpic interaction that particle clusters can be dispersed via the formation of distinct bound layers on different fillers. Furthermore, because of the polymeric nature of the chain, a small change in the *per segment* enthalpic contribution can result in a substantial amount of steric stabilization. These two effects combine to render the location of the F + F phase boundary relatively insensitive to nanoparticle size. In contrast, the phase boundary separating the miscible state from the networked phase not only occurs much more gently (i.e., over a much broader range of monomer−filler attraction strength), but also shows a marked shift toward less miscibility with increasing particle size. Here, the ability of the particle size to affect the phase diagram is attributed to the enhanced polymer-bridging interactions that can be realized with increasingly larger (and hence, locally flatter) filler surfaces.[20]

The effect of increasing polymer chain length has also been studied and contrasted with the consequences of increasing D/d. Qualitative trends similar to those found with increasing particle size occur, as demonstrated in Figure 7 for a wide range of $N = 25-1600$. As chains get larger and lose translational entropy, the miscibility window narrows, although the quantitative magnitude of the effect is much less than that found for increasing nanoparticle size. The F + F boundary remains sharp and stable in ϵ_{pc} value for the same qualitative reasons as discussed above. The network phase boundary does systematically shift in the direction of less miscibility as chain degree of polymerization increases. The reason for the much weaker dependence on N compared to D/d is that, when the system organizes into a bridging configuration, it does so on the local segmental length scale.[20] Because the dense polymer matrix is dominated by effects that occur at the polymer mesh size, which is nearly independent of chain length,[21,32] a zeroth-order expectation would be that chain size should have no effect on the networked phase boundary. However, a networked phase occurs because of packing near (and packing distortions due to the presence of) the particle surface and their subsequent effects on the attractions generated between nanoparticles. We have previously shown the net effect of increasing chain size leads to somewhat larger repulsive barriers in the PMF and slightly increased attractive well depths at the global (deepest) minimum and also deeper PMF minima at larger interfiller separations.[20] Such trends are physically intuitive and consistent with our prediction of a modest enhancement of the stability of the networked phase.[20] This chain length dependence is a finite size effect in the sense that the PMF and phase boundaries approach limiting values for large N.

An interesting consequence of the above N dependence is that, for a fixed material, the networking phase transition can potentially be induced by increasing degree of polymerization. Realization of this trend does require values of the monomer−filler attraction energy in a rather narrow range. Measurements of a network-type phase separation, or perhaps its nonequilibrium analogue gelation, could probe this effect. Most directly relevant within the context of our present work would be measurements of the N-dependence of the second virial coefficient. At the rather large values of ϵ_{pc} relevant to the networking transition, the second virial coefficient decreases with N (ultimately saturating), and near the onset of the network transition perhaps could be observed to even change sign with increasing chain length.

B. Chemistry-Related Effects. The controlling chemical or material-specific variables of a polymer nanocomposite is the effective contact cohesive energy per segment, ϵ_{pc}, and the spatial range of the monomer−particle attraction.[20] Figure 8 illustrates the role of interfacial attraction range on the phase diagrams. The F + F boundary monotonically shifts to lower values of ϵ_{pc} with increasing attraction range. This trend reflects the enhanced interfacial cohesion associated with a larger value of α.

A complex nonmonotonic dependence on spatial range exists for the networked phase spinodal curves at high ϵ_{pc}. The narrowest miscibility window is associated with the shortest-range interaction ($\alpha = 0.25$) due to the strong bridging tendency of this system at large monomer−particle adsorption energies. However, the next smallest miscibility window is not for the $\alpha = 0.5$ system (the next-strongest bridging system at moderate values of ϵ_{pc}), but rather the longer-range or "softer" attraction system ($\alpha = 1.0$). This is due to an inversion of the relationship

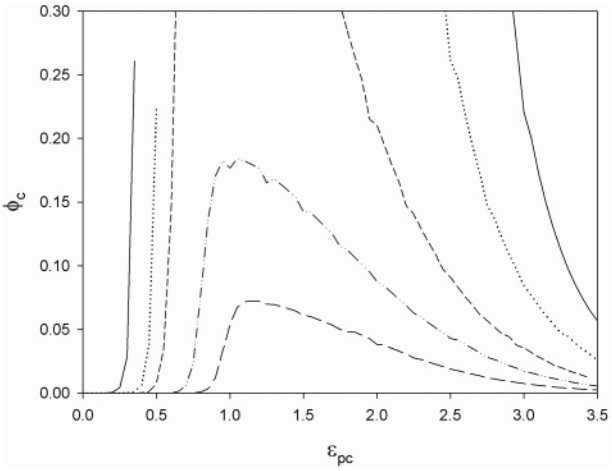

Figure 9. Nanoparticle volume fraction at the spinodal as a function of interfacial attraction for sticky particles with $D/d = 16$, $N = 100$ and $\alpha = 0.5$. Calculations are shown for $\beta\epsilon_{cc} = 0$ (solid), 5.0 (dotted), 10.0 (short dash), 15.0 (dash−dot−dot), and 20.0 (long dash).

between the values of α and the minimum in the PMF at high ϵ_{pc}.[20] While smaller values of α generally lead to larger attractive (bridging) wells in the PMF at low to moderate values of ϵ_{pc}, this trend reverses at high values of ϵ_{pc} due to the deep attractive wells that result from the transition from steric stabilization to telebridging configurations for $\alpha = 1$.[20] For such high per-segment adsorption energies due to the already highly compressed bound layer near the nanoparticle surface, the magnitude of the attraction between nanoparticles becomes very large with small incremental increases in ϵ_{pc}, causing the shift of the network formation curve to cross the $\alpha = 0.5$ system spinodal boundary. In fact, at the highest values of ϵ_{pc} investigated, the $\alpha = 1.0$ telebridging[20] is even stronger than the tightly bridged $\alpha = 0.25$ system, as can be seen in the inset of Figure 8. Hence, the window of miscibility at relatively low filler volume fractions is widest for the $\epsilon_{pc} = 0.5$ system due to a subtle balance of bridging and steric stabilization contributions to the free energy of mixing, which efficiently frustrates the formation of the network phase.

V. Effect of Direct Filler Attractions on Miscibility

To gain a feeling for the consequences of direct, dispersive, or van der Waals attractions between particles, the CLJ potential model[20,22] has been utilized to address two different questions. For one series of calculations, all system variables are fixed except the overall attraction between fillers at contact, ϵ_{cc}, which allows the effect of increasing interfiller cohesion on the miscibility window to be deduced. In practice, ϵ_{cc} increases with the magnitude of the dielectric contrast between polymer and fillers and the nanoparticle diameter. Figure 9 shows results for $0 \le \epsilon_{cc} \le 20\ k_BT$. As expected, as the strength of the direct attraction between particles is increased, the miscibility window shrinks. As $\epsilon_{cc} \rightarrow 15\ k_BT$, there is a clear maximum of the miscibility window at $\epsilon_{pc} \approx 1.0-1.5$ corresponding to an interfacial energy range which best frustrates the direct contact aggregation that controls the location of the F + F phase boundary while minimizing the bridging mechanism that induces the networked phase. The slight shift of the location of this optimally miscible state to higher ϵ_{pc} as ϵ_{cc} increases is due to the enhanced shift of the F + F phase boundary brought about by the direct attraction.

As pointed out in eq 4, the magnitude of the direct van der Waals attraction scales linearly with nanoparticle size. For real materials with constant constituent *chemistry*, rather than

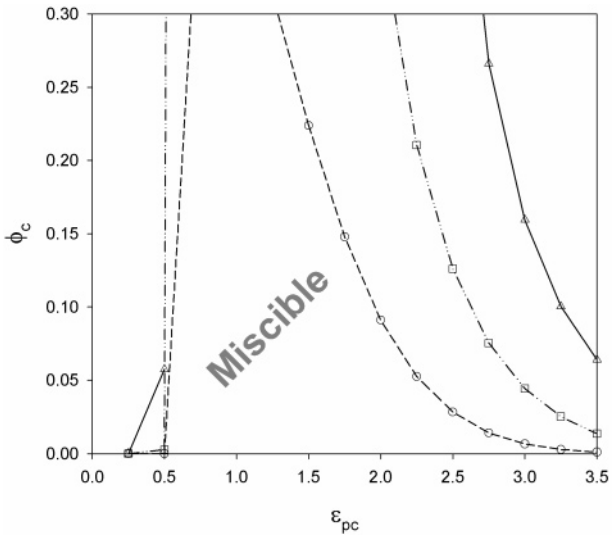

Figure 10. Effect of nanoparticle size on spinodal boundaries for sticky particles and fixed system chemistry, $N = 100$ and $\alpha = 0.5$. The reference system corresponds to ϵ_{cc}^0 and $D_0 = 24d$. Results are shown for $D/d = 24$ (D_0, circle), 16 (0.66 D_0, square), and 10 (0.42 D_0, triangle).

constant net interaction, this scaling of attraction with nanoparticle size will play an important role in exacerbating phase-separation tendencies as the size asymmetry ratio D/d increases. Introducing a reference system, this D/d scaling corresponds to:

$$\frac{\epsilon_{cc}^{eff}}{\epsilon_{cc}^{0}} = \frac{D_{eff}}{D^0} \tag{25}$$

where ϵ_{cc}^0 and D^0 represent the reference state values, and ϵ_{cc}^{eff} is the net direct attraction at contact of a chemically identical particle of diameter D_{eff}. As can be seen in Figure 10, when direct nanoparticle attractions are included, there is a tendency for smaller particles to undergo a network-type phase separation at higher interfacial energies. On the other hand, the initial onset of miscibility at low ϵ_{pc} is again only weakly sensitive. This is analogous to the trends in Figure 6 and reflects the reduced cohesion associated with bridging as fillers get smaller.

VI. Discussion and Summary

PRISM theory has been employed to compute the second virial coefficients (B_2) of hard-sphere nanoparticles dissolved in polymer melts for a wide variety of monomer−filler attractive interactions that mimic the highly nonuniversal chemical aspects of real polymer nanocomposites. A generic finding is an attractive(depletion)-to-repulsive(sterically stabilized)-to-attractive(local bridging) transition of B_2 with increasing interfacial contact cohesion strength, ϵ_{pc}. Direct nanoparticle attractions can greatly modify the breadth of each region of this transition depending on the spatial range of the interfacial attraction. In particular, for the shorter-range attraction ($\alpha = 0.25$), second virial coefficients display little repulsive character. On the other hand, for the longest-range attraction ($\alpha = 1.0$), B_2 remains repulsive over the majority of ϵ_{pc} values investigated. Polymer chain length plays little role for weak monomer−particle attractions where the contact depletion attraction mechanism dominates. However, for bridging-induced attraction, the second virial coefficient decreases with increasing degree of polymerization. As the network-like phase-separation boundary is approached, values of ϵ_{pc} must exist such that increasing N can

result in B_2 changing from repulsive (positive) to attractive (negative). These virial coefficient predictions are potentially measurable using small-angle X-ray scattering.[39]

Utilizing either an effective one-component model based solely on B_2 or the rigorous perturbative in filler concentration approach, PRISM theory predicts two distinct spinodal demixing curves, separated by a "miscibility window", for all combinations of the materials parameters investigated. One demixing curve is encountered at relatively low attraction strength ($\epsilon_{pc} \leq 1\ k_BT$) and represents a very abrupt transition from an entropic depletion-induced demixed system composed of polymer-rich and nanoparticle-rich phases to a miscible fluid. The transition to a miscible fluid is enthalpically triggered by the formation of thermodynamically stable bound polymer layers around fillers. Such layers result in an increase of the effective particle diameter and interparticle repulsions via a steric stabilization-type mechanism. The location of this spinodal boundary is relatively insensitive to nanoparticle size asymmetry ratio (D/d) and interfacial attraction range (α).

The second demixing transition occurs at relatively high monomer−particle adsorption energy and signals the dominance of enthalpic effects in the free energy of mixing. On the basis of the nanoparticle potentials of mean force in the infinite dilution limit,[20] we infer its physical nature is the formation of a thermodynamically stable networked phase where fillers are locally bridged by polymer chains. This spinodal boundary is more sensitive to both D/d and α, with increases of either resulting in a narrowing of the range of parameter space over which miscibility occurs. Hence, experimental realization of the predicted thermodynamic miscibility and associated excellent dispersion requires both an intermediate value of ϵ_{pc} and modest-sized fillers (nanoparticles). In all cases, a narrowing of the miscibility window is associated with increased bridging between nanoparticles. As a consequence, the miscibility window is also predicted to quantitatively narrow with increasing polymer chain length. This is a finite size effect with a well-defined long-chain limiting behavior due to the fundamentally local nature of the relevant bridging configurations in a dense, nearly incompressible melt.

Phase separation where the spatial organization of one of the coexisting phase is a dense interpenetrating network or complex is commonly observed in polyelectrolyte solutions, especially for biopolymer systems such as lipid−DNA or lipid−actin mixtures.[40,41] However, the analogous phase transition for polymer nanocomposites in the melt state is likely very difficult to realize in the laboratory due to slow kinetics. Instead, the thermodynamic desire to form polymer−particle complexes or networks likely triggers nonequilibrium gelation. Indeed, such a phenomenon presumably underlies the often spectacular enhancement of the rubbery elastic modulus of polymer melts and elastomers upon addition of fillers.[1−4]

Direct van der Waals attractions between fillers result in a narrowing of the miscibility window. As the direct nanoparticle attraction strength at contact (ϵ_{cc}) is increased, the miscibility window can eventually disappear. If, instead, the chemistry of the system is held constant and the particle size increased, a similar destruction of the miscibility window is seen for increasing size asymmetry ratio, D/d.

The existence of a miscibility window for intermediate filler−polymer attractions and small or moderate direct van der Waals interactions is a major new prediction. We hope it will help guide the synthesis and/or formulation of novel thermodynamically stable polymer nanocomposites with excellent dispersion. Realization of such a homogeneous polymer nanocomposite is predicted to require nanosized fillers rather than traditional micron-sized particles. As previously discussed,[20] even for cases where thermodynamic phase separation is expected, kinetic stabilization and particle dispersion due to large repulsive barriers in the filler potential of mean force is also possible in analogy with the classic case of stable sticky charged colloidal suspensions.[24]

Ongoing theoretical work is employing PRISM theory to determine phase diagrams and structure at nonzero filler volume fractions. Novel predictions in the miscible phase for both the collective polymer and filler structure factors at both small and large angles have been obtained that are amenable to testing using X-ray and/or neutron scattering.[42] Computational studies of the three coupled nonlinear integral equations, from which spinodal boundaries based on the full theory at finite filler volume fraction follow, are also under study. However, for parameter values where phase separation is expected from the virial-like analysis, we encounter extreme difficulties with numerical convergence that render such calculations very difficult at present. Not surprisingly, preliminary results do find differences with respect to the virial-based phase boundaries. However, these differences are only quantitative in nature and appear to often be of modest magnitude. Generalization of the theory to treat more complex fillers such as rods, disks, deformable microgels, and nanoparticles coated with grafted chains is a major direction of ongoing and future work.

Acknowledgment. This work was supported by the Nanoscale Science and Engineering Initiative of the National Science Foundation under NSF Award no. DMR-0117792, and Oak Ridge National Laboratory via the Division of Materials Science of the Department of Energy. Discussions and/or correspondence with S. K. Kumar, Ben Anderson, and Chip Zukoski are gratefully acknowledged.

References and Notes

(1) Wang, M.-J. *Rubber Chem. Technol.* **1998**, *71*, 520; **1999**, *72*, 430.
(2) Huber, G.; Vilgis, T. A. *Macromolecules* **2002**, *35*, 9204.
(3) Vieweg, S.; Unger, R.; Heinrick, G.; Donth, E. *J. Appl. Polym. Sci.* **1999**, *73*, 495.
(4) Ajayan, P. M.; Schadler, L. S.; Braun, P. V. In *Nanocomposite Science and Technology*; Wiley-VCH: Weinheim, 2003; p 77.
(5) Ash, J.; Schadler, L. S.; Siegel, R. W. *Mater. Lett.* **2002**, *55*, 83.
(6) Mackay, M. E.; Dao, T. T.; Tuteja, A.; Ho, D. L.; van Horn, B.; Kim, H.-C.; Hawker, C. J. *Nat. Mater.* **2003**, *2*, 762.
(7) Patel, R.; Egorov, S. A. *J. Chem. Phys.* **2004**, *121*, 4987; **2002**, *123*, 144916.
(8) Salaniwal, S.; Kumar S. K.; Douglas, J. F. *Phys. Rev. Lett.* **2002**, *89*, 258301.
(9) Starr, F. W.; Schroeder, T. B.; Glotzer, S. C. *Macromolecules* **2002**, *35*, 4481; *Phys. Rev. E* **2001**, *64*, 021802.
(10) Starr, F. W.; Douglas, J. F. *J. Chem. Phys.* **2003**, *119*, 1777.
(11) Vacatello, M. *Macromolecules* **2001**, *34*, 1946; **2002**, *35*, 8191.
(12) Smith, J. S.; Bedrov, D.; Smith, G. D. *Compos. Sci. Technol.* **2003**, *63*, 1599.
(13) Bedrov, D.; Smith, G. D.; Smith, J. S. *J. Chem. Phys.* **2003**, *119*, 10438.
(14) Desai, T.; Keblinski, P.; Kumar, S. K. *J. Chem. Phys.* **2005**, *122*, 134910.
(15) Yethiraj, A.; Hall, C. K.; Dickman, R. *J. Colloid Interface Sci.* **1992**, *151*, 102.
(16) Dickman, R.; Yethiraj, A. *J. Chem. Phys.* **1994**, *100*, 4683.
(17) Khalatur, P. G.; Zherenkova, L.; Khoklov, A. R. *Physica A* **1997**, *247*, 205.
(18) Schweizer, K. S.; Curro, J. G. *Adv. Chem. Phys.* **1997**, *98*, 1; Curro, J. G.; Schweizer, K. S.; Grest, G. S.; Kremer, K. *J. Chem. Phys.* **1989**, *91*, 1357; Honnell, K.; Curro, J. G.; Schweizer, K. S. *Macromolecules* **1990**, *23*, 3496.
(19) Hooper, J. B.; Schweizer, K. S.; Desai, T. G.; Koshy, R.; Keblinski, P. *J. Chem. Phys.* **2004**, *121*, 6986.
(20) Hooper, J. B.; Schweizer, K. S. *Macromolecules* **2005**, *38*, 8858.

(21) Doi, M.; Edwards, S. F. In *Theory of Polymer Dynamics*; Oxford University Press: New York, 1986.
(22) Henderson, D.; Duh, D. M.; Chu X.; Wasan, D. *J. Colloid Interface Sci.* **1997**, *185*, 265.
(23) Israelachvili, J. In *Intermolecular and Surface Forces*; Academic: London, 1997.
(24) Russel, W. B.; Saville, D. A.; Schowalter, W. R. In *Colloidal Dispersions*; Cambridge University Press: New York, 1989.
(25) Chen, Y. L.; Fuchs, M.; Schweizer, K. S. *J. Chem. Phys.* **2003**, *118*, 3880.
(26) Fuchs, M.; Schweizer, K. S. *J. Phys: Condens. Matter* **2002**, *14*, R239.
(27) Fuchs, M.; Schweizer, K. S. *Europhys. Lett.* **2000**, *51*, 621.
(28) Fuchs, M.; Schweizer, K. S. *Phys. Rev. E* **2001**, *64*, 021514.
(29) Ramakrishnan, S.; Fuchs, M.; Schweizer, K. S.; Zukoski, C. F. *J. Chem. Phys.* **2002**, *116*, 2201.
(30) Shah, S. A.; Chen, Y. L.; Schweizer, K. S.; Zukoski, C. F. *J. Chem. Phys.* **2003**, *118*, 3350.
(31) Shah, S. A.; Chen, Y. L.; Schweizer, K. S.; Zukoski, C. F. *J. Phys.: Condens. Matter* **2003**, *15*, 4751.
(32) Koshy, R.; Desai, T. G.; Keblinski, P.; Hooper, J.; Schweizer, K. S. *J. Chem. Phys.* **2002**, *117*, 1893.
(33) Chandler, D.; Andersen, H. C. *J. Chem. Phys.* **1972**, *57*, 1930; Chandler, D. In *Studies in Statistical Mechanics*; Montroll, E. W., Lebowitz, J. L., Eds.; North-Holland: Amsterdam, 1982; p 274.
(34) Hansen, J. P.; McDonald, I. R. In *Theory of Simple Liquids*; Academic: London, 1986.
(35) George, A.; Wilson, W. *Acta Crystallogr. D* **1994**, *50*, 361.
(36) Rosenbaum, D. F.; Zamora, P. C.; Zukoski, C. F. *Phys. Rev. Lett.* **1996**, *76*, 150.
(37) Rosenbaum, D. F.; Zukoski, C. F. *J. Crystal Growth* **1996**, *169*, 752.
(38) Kulkarni, A. M.; Chatterjee, A. P.; Schweizer, K. S.; Zukoski, C. F. *Phys. Rev. Lett.* **1999**, *83*, 4554.
(39) Anderson, B.; Zukoski, C. F. private communication.
(40) Koltover, I.; Salditt, T.; Radler, J. O.; Safinya, C. R. *Science* **1998**, *281*, 78; Wong, G. C. L.; Tang, J. X.; Lin, A.; Li, Y.; Janmey, P. A.; Safinya, C. R. *Science* **2000**, *288*, 2035.
(41) Tang, J. X.; Janmey, P. A. *J. Biol. Chem.* **1996**, *271*, 8556.
(42) Hooper, J. B.; Schweizer, K. S. in preparation.

MA060577M